A PRELIMINARY COMPARISON OF TWO EXCLUSION MAPS FOR LARGE-SCALE FLOOD MAPPING USING SENTINEL-1 DATA

Jie Zhao[1], Florian Roth[2], Bernhard Bauer-Marschallinger[2], Wolfgang Wagner[2], Marco Chini[3], and Xiao Xiang Zhu[1]

[1]Chair of Data Science in Earth Observation, Technical University of Munich, Arcisstraße 21, Munich 80333, Germany
[2]Department of Geodesy and Geoinformation, TU Wien, Wiedner Hauptstr 8, Vienna A-1040, Austria
[3]Department of Environmental Research and Innovation, Luxembourg Institute of Science and Technology, 5 Avenue des Hauts-Fourneaux, Esch-sur-Alzette 4362, Luxembourg

KEY WORDS: SAR, flood mapping, exclusion map, insensitive

ABSTRACT:

Due to its ability to acquire data regardless of weather conditions and solar illumination, Synthetic Aperture Radar (SAR) intensity data is the preferred data for large-scale flood mapping. However, due to the SAR image distortions and complex land cover conditions at large scale, there are areas where SAR data is unable to measure ground surface changes caused by floodwater, which is crucial information that cannot be overlooked for large-scale applications. To address this limitation of SAR data, two similar products, the LIST Exclusion map (EX-map) and the GFM exclusion mask, were recently proposed to identify these problematic areas. As there is no established criterion to evaluate these two products, a comprehensive comparison is necessary to investigate the consistency and differences between them for different end-users' needs. We conducted the first-ever comparison between the LIST EX-map and the GFM exclusion mask, from their definitions to the site-scale products, while elaborating on their preferred application domains for different algorithms. We qualitatively and quantitatively evaluated the exclusion map using Sentinel-1 data for 11 test sites across five continents with global land cover maps to identify the advantages and disadvantages of both approaches. The results show that the main differences exist in mountainous radar layovers/shadows and low vegetation such as grass, cropland, and shrubland. The evaluation results demonstrate a good agreement (64.87% $\sim$ 91.40%) between the two products.

1. INTRODUCTION

Synthetic Aperture Radar (SAR) data has found widespread application in various domains, including flood mapping, soil moisture retrieval, and glacier monitoring, owing to its ability to detect changes in the ground surface despite sun illumination and weather conditions. While SAR is able to provide valuable information about soil moisture, vegetation cover, and other surface properties, there are certain scenarios where SAR backscatter remains insensitive to changes in the ground surface. As summarized in (Zhao et al., 2021):

- The layover in SAR images, which is a result of the side-looking geometry of SAR sensors, is insensitive to the surface features as the reflected SAR signal from the tops of objects appears to be displaced from their base, leading to high backscatter. In contrast, changes in backscatter caused by variations in the ground surface are too small to be detected compared to the extremely high backscatter caused by layover.
- Double bouncing areas, in particular those areas in urban, cause very high backscatter and result in insensitivity as well.
- Shadow areas are also insensitive areas since the SAR signal cannot reach the ground surface due to obstacles and no information could be retrieved.
- Dense vegetated areas may be another kind of insensitive area depending on the wavelength of SAR signal. L-band SAR signal is able to penetrate through dense vegetation canopy while X-band and C-band SAR is only able to obtain the information from the vegetation canopies.
- Dry sands/arid areas with smoother surfaces have stable low backscatter over time which is difficult to be distinguished from flooded conditions.

Numerous flood mapping investigations have concentrated on particular locations, resulting in a lack of comprehensive analysis on the majority of the aforementioned phenomena. A limited number of studies, such as those conducted by (Martinis et al., 2018, Benoudjit and Guida, 2019, Bauer-Marschallinger et al., 2022), have proposed auxiliary data usage or devised customized masks tailored to their respective objectives. Nevertheless, the feasibility of applying such methodologies to facilitate large-scale flood mapping remains uncertain.

To address the issue of insufficient sensitivity in low-sensitivity regions of Synthetic Aperture Radar (SAR) data for large-scale flood mapping, two recent approaches have emerged. The first approach is a decision-tree-based EX-map proposed by (Zhao et al., 2021), which uses three multi-temporal indicators to systematically identify insensitive areas. The second approach is an exclusion mask that encompasses all insensitive areas developed by the Copernicus Global Flood Monitoring (GFM) service (Salamon et al., 2021). The GFM aims to provide systematic and continuous global flood monitoring by immediately processing and analyzing Sentinel-1 Interferometric Wide Swath data. In addition to the GFM exclusion mask, GFM products provide accurate binary flood maps generated by integrating three independently developed flood mapping algorithms with probabilistic flood maps indicating uncertainty, an advisory flag indicating potentially reduced quality of flood mapping due to meteorological conditions or degraded input data quality, a Sentinel-1 derived reference water mask, and information on flood-affected population and land cover.

This contribution has been peer-reviewed. The double-blind peer-review was conducted on the basis of the full paper.
https://doi.org/10.5194/isprs-annals-X-1-W1-2023-911-2023 | © Author(s) 2023. CC BY 4.0 License.

Although both techniques use time-series Sentinel-1 C-band data to generate insensitive regions, there are differences in the methodology employed and the significance of the information produced. Furthermore, there is no definitive criterion for evaluating the effectiveness of both exclusion layers. Therefore, a comprehensive comparative analysis is needed to investigate the consistency of the two products for end-users with diverse requirements.

The study aimed to evaluate the consistency between the LIST EX-map proposed by (Zhao et al., 2021) and the GFM exclusion mask. The comparison of the two products was conducted at 11 study sites, accounting for various surface conditions and climates. To get a better understanding of the land cover classes of inconsistencies, multi-source reference data was also utilized. The evaluation aimed to identify the problematic areas between the two global exclusion layers and provided users with a clear understanding of their consistency, as well as potential directions for improvement. The remaining sections are organized as follows: Section 2 outlines the definitions and methodology of both exclusion maps, section 3 introduces the experimental materials, including datasets, study sites, and comparison methods, section 4 presents the results and associated discussions, and section 5 summarizes the analysis's conclusion.

2. EXCLUSION MAP GENERATION

2.1 LIST EX-map generation

The LIST EX-map proposed by (Zhao et al., 2021) defines areas that cannot be reliably classified as 'flooded' or 'not flooded' using SAR intensity data. The EX-map is expected to include five SAR-based categories according to this definition: 1) permanent water bodies; 2) shadow (topographic, urban), and arid areas; 3) layover (topographic); 4) layover/double bounce (urban); and 5) densely vegetated areas. The EX-map's definition is based on a general assumption that areas with permanently low and high backscattering values, as well as areas with stable backscattering over time, should be excluded when mapping floodwater using only SAR intensity information. Thus, the LIST EX-map is defined by three components: low backscattering (LB) class, high backscattering (HB) class, and stable backscattering (SB) class. In order to classify these three classes, three multi-temporal indicators are proposed: multi-temporal minimum (Min_{TM}), multi-temporal standard deviation (σ_{TM}), and standardized local Getis-Ord G_i (referred to as local G_i), calculated based on the multi-temporal median image of time-series SAR intensity data. The decision tree-based EX-map generation method follows this workflow:

1. **HB** includes pixels with extremely high local G_i, including topographic layover and layover/double-bounce effect pixels in urban.
2. **LB** includes pixels with extremely low local G_i, including permanent water bodies, topographic shadow and the 'water-lookalike areas' (e.g., arid areas, airport and tarmac). In this LB class, permanent water bodies can be distinguished from topographic shadow and the 'water-lookalike areas' as it has higher σ_{TM} compared with the latter;
3. **SB** includes pixels with moderate local G_i, low σ_{TM} and high Min_{TM}, including the dense vegetation only.

It is noteworthy that the HSBA algorithm (Chini et al., 2017), which is an automatically adaptive thresholding method, was utilized. The HSBA algorithm was initialized and constrained using empirical-based prior values. For instance, the initial value of local G_i for HB and LB classification was set at 5 and -5, respectively. The threshold of σ_{TM} for SB was fixed at 2 dB, and the initial value of Min_{TM} was chosen as -15 dB.

2.2 GFM Exclusion mask

The GFM Exclusion mask described in (GFM, 2022) is defined as the pixel locations where SAR data could not deliver the necessary information for a robust delineation, due to the combined effects of the following 'static' factors: no sensitivity in flood mapping (i.e., dense vegetation and urban areas), permanent low backscatter creating 'water-look-alike' (i.e., flat and impervious areas, sandy surfaces, permanent water bodies) and strong topography and radar shadows (i.e., topographic effects). Thus, the exclusion mask is generated based on the offline-generated Sentinel-1 SAR parameters and auxiliary thematic dataset as following:

1. **Non-sensitivity** includes dense vegetation and urban areas. Dense vegetation was identified using parameters from the Sentinel-1 Global Backscatter Model (S1GBM) (Bauer-Marschallinger et al., 2021), including spatially harmonized mean backscatter values in VV and VH polarization, mean cross-polarization ratio, and standard deviation in VH polarization. Pixels were classified as dense vegetation if they displayed relatively high mean backscatter in VV polarization, relatively low mean backscatter in VH polarization, a relatively high mean cross-polarization ratio, and a relatively high standard deviation in VH polarization. For this part of the analysis, thresholds were independently optimized for each continent and varied based on latitude and vegetation type. Meanwhile, urban mask was derived from the Global Human Settlement Layer (GHSL) (JRC, 2021) and World Settlement Footprint (WSF2015) (Marconcini et al., 2020) static urban masks. It is defined as pixels with a GHS-BUILD value greater than 30% and belonging to WSF2015.
2. **Low backscatter areas** include pixels where the occurrence of low backscatter values (below –15 dB) exceeds 70% of the corresponding time-series (Martinis et al., 2018).
3. **Topographic distortions** are identified by applying a mask for pixels with HAND-values higher than 15m, thus also effectively masking locally elevated areas that are not prone to be flooded (Chow et al., 2016).
4. **Sentinel-1 radar shadows** are defined as pixels with a temporal mean backscatter less than -15 dB in current orbit while its mean backscatter value in opposite direction is higher than -10 dB. This allows masking shadows not only in rough terrain but also along forest lines or other non-terrain radar shadows.

3. EXPERIMENTAL MATERIALS

3.1 Study sites and dataset

To facilitate the evaluation of exclusion maps, 11 representative study sites were selected from 5 continents (Figure 1), taking into account diverse land cover classes, topographic conditions, and climates. To ensure a fair comparison of the exclusion maps, the same time-series Sentinel-1 data was utilized for

both. As the GFM exclusion mask was created using only two years of Sentinel-1 time-series data (2019-2020) from TU Wien Data Cube (Wagner et al., 2021), the LIST EX-map was also produced using the same two years of Sentinel-1 time-series data. All data was geocoded and processed into tiles of 300 × 300 km^2 with a spatial resolution of 20 m. Similar to (Zhao et al., 2021), a multi-source reference was generated based on the definition of exclusion maps, including:

1. 30m FROM-GLC map derived from optical data (Gong et al., 2013)
2. shadow/layover mask generated by DEM simulator and SAR acquisition geometry of each orbit tracks used in this study (Kropatsch and Strobl, 1990)
3. 10m resolution World Settlement Footprint (WSF) 2019 data provided by (Marconcini et al., 2021)
4. 20m resolution Sand Exclusion Layer (SEL) generated by (Martinis et al., 2018)

It is worth noting that the SEL is only considered in the study site of Beledweyne (Somalia) and Iran since both study sites cover areas which are classified as hot deserts with arid conditions in the Köppen climate classification system (Peel et al., 2007).

Figure 1. Selected study sites from five continents.

3.2 Evaluation method

A two-step comparison strategy was adopted. First, the definitions of the two products were compared. Then, the multi-source evaluation reference map was employed to evaluate both exclusion maps in order to have a better understanding of the land cover types of all pixels included. Meanwhile, the cross-validation between both exclusion maps was carried out. The comparison was implemented at 11 study sites (Figure 1) from 5 continents, covering arid areas, vegetated regions and mountainous zones.

4. RESULTS AND ANALYSIS

4.1 Comparison in Definitions

As described in section 2, both products have several similar sublayers but with different definitions. Table 1 summarised and compared those similar sublayers between those two products: 1) for the layover areas and urban areas, LIST EX-map identifies pixels with extremely high backscatter over time, making it difficult to distinguish them apart without auxiliary data. The GFM exclusion mask provides non-flood-prone areas derived from HAND index, covering all the topographic layover and topographic shadow pixels and also other areas in mountainous regions. The urban mask from GFM exclusion mask covers all the settlement areas from other sources while LIST EX-map only identifies the urban pixels having layover or double-bounce effects; 2) Similarly, topographic shadow, arid areas, airports, motorways and permanent water bodies are classified as a single-layer with extremely low backscatter in LIST EX-map, where permanent water bodies can be separated from the rest using its high variance in backscatter over time due to the wind. In the GFM exclusion mask, low backscatter areas are defined by multi-temporal backscatter while radar shadow, including forest edges and riparian areas, is separated using the differences among the opposite orbit pass directions; 3) The dense vegetation in LIST EX-map is defined as vegetation with stable backscatter over time and relatively higher multi-temporal minimum backscatter. However, the dense vegetation in GFM exclusion mask is defined as areas having high biomass areas such as forests and shrubland with biomass levels larger than 30-50 t/ha (Quegan et al., 2000), considering both VV and VH Sentinel-1 polarization data.

Due to these different definitions, the input data for each product is also different: LIST EX-map relies on a single data source, i.e., 2 years time series Sentinel-1 data acquired in VV polarization; GFM exclusion mask requires 2 years time series Sentinel-1 data acquired VV and VH polarization and also the two static urban masks (i.e., GHSL, WSF2015), S1GBM and HAND index. Moreover, it should be noted that the three layers of the LIST EX-map are orbit-dependent while the radar shadow of the GFM exclusion mask is the only orbit-dependent layer.

4.2 Comparison among both exclusion maps and reference map

As defined in section 3.1, the reference map includes 14 classes: 10 land cover classes from FROM-GLC map, shadow and layovers for SAR simulator, WSF2019 and SEL. According to the definition of exclusion maps, seven classes should be covered by exclusion maps theoretically: forest, water, impervious surface, layover, shadow, WSF2019 and SEL. However, it should be noted that in the following analysis, LIST EX-map is compared with the GFM exclusion map only including dense vegetation, urban mask, non-water low backscatter areas and Sentinel-1 radar shadow without considering the topographic distortions since it removes quite large mountainous regions not only the topographic shadow layover but also other vegetated areas. Then, the analysis of those seven classes in the LIST EX-map and the GFM exclusion mask was carried out and results are listed in Table 2, indicating that an agreement between two exclusion maps can be found. However, the agreement between each exclusion map with reference map is relatively low, especially for the two study sites located in Somalia and Iran respectively.

Figure 2 displays large areas classified as shrubland and bareland in both exclusion maps based on the FROM-GLC map in Somalia and Iran, respectively. More specifically, shrubland in Somalia with stable moderate backscatter over time are always classified as dense vegetation in LIST EX-map and GFM exclusion mask. Similar phenomenon in bareland is observed in the study site in Iran. Although the significant difference between

exclusion maps and reference map is acceptable due to different definitions of reference map used here, further investigation should be carried out in the future for the arid study sites to find strong evidence of whether shrublands and bareland should be regarded as SAR insensitive areas or not.

Table 1: Comparison of the sublayers of both exclusion maps (similar sublayers are shown in the same color)

LIST EX-map		GFM exclusion mask	
Layers	Sublayers	Layers	Sublayers
High backscatter region (i.e. HB)	Topographic Layover		Dense vegetation
	Urban (layover, double-bounce effect)	No-sensitivity	urban mask
Low backscatter region (i.e. LB)	Permanent water bodies	Low backscatter	Airport + motorways + sandy surface + Permanent water bodies
	Topographic shadow & Arid areas + airport + tarmacs	Sentinel-1 radar shadows	Radar shadow
Stable backscatter region (i.e. SB)	Dense vegetation	Topographic distortions	Non-flood prone areas (including topographic layover/shadow)

Table 2: Overall accuracy of each exclusion map using the reference map as ground truth

Study sites	Orbit	LIST EX-map	GFM exclusion mask
Severn, UK	30	54.97%	56.07%
	154	52.25%	55.50%
Milan, Italy	15	73.96%	72.95%
	66	67.10%	67.47%
Beledweyne, Somalia	35	7.12%	5.45%
Beijing,China	47	43.12%	67.72%
Wuhan,China	113	64.44%	70.02%
Houston, US	34	79.88%	83.68%
Iran	35	29.31%	57.51%
Ecuador	18	61.28%	69.08%
Hungary	175	65.16%	69.86%
Mexico	34	69.21%	59.58%
Mexico	99	69.82%	61.86%
Myanmar	143	59.14%	61.97%

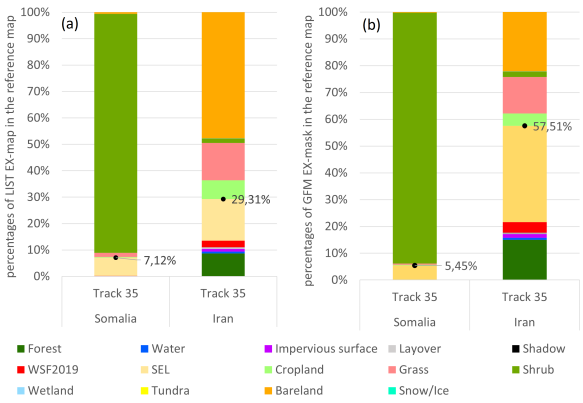

Figure 2. Detailed analysis for Somalia and Iran cases of specific orbit-based exclusion maps: (a) Land cover classes of pixels included in the LIST EX-map; (b) Land cover classes of pixels included in the GFM exclusion mask.

4.3 Detailed analysis for representative study sites

In order to have a better understanding of two exclusion maps, the agreement and disagreement between them are analyzed. The disagreement is discussed in detail using the reference map. Figure 3 depicts the agreement and disagreement between LIST EX-map and GFM exclusion mask. The agreement ranges from 64.87% to 91.40% indicating a good agreement between two products when it comes to such large areas of coverage. Furthermore, Figure 4 shows the land cover classes of those disagreement areas in LIST EX-map and GFM exclusion mask. The exclusion map should ideally comprise the land cover classes that are stacked below the black point in each column bar of the figure, along with their cumulative percentages. On the other hand, the land cover classes that SAR is expected to be sensitive to changes in ground surfaces are depicted above the black point in each column bar. In the following, several representative study sites discussed in detail, including Severn (UK), Milan (Italy), Beijing (China), Iran and Ecuador.

4.3.1 Study site: Severn, UK In this study site, the LIST EX-map and GFM exclusion mask showed a good agreement with an overall accuracy of 91.4%. Differences between the products were mainly observed in the boundaries of urban, cropland, road, and forest areas, as illustrated in Figure 5. The red pixels in Figure 5 (b) highlight the radar shadow of trees in the GFM exclusion mask, indicating that the LIST EX-map may not have included the shadows of trees and forest. The blue pixels in Figure 5 (d) represent built-up areas that were included in the LIST EX-map but were misclassified in the no-sensitivity layer of the GFM exclusion mask.

4.3.2 Study site: Milan, Italy In this study site, the main sources of disagreement come from the mountainous areas classified as grassland in the reference map belonging to radar layover and shadows are not well identified. In particular, LIST EX-map includes more pixels as topographic layovers (blue pixels in Figure 6) which could be all covered by the topographic distortion mask from the GFM exclusion mask. However, GFM exclusion mask identifies more pixels as Sentinel-1 radar shadow and also dense vegetation as shown in red in Figure 6. The backscatter distributions of shadow areas provided by LIST EX-map and GFM exclusion mask are displayed in Figure 6 (f), pointing out that the difference comes from the different definitions of the two products. In particular, while LIST

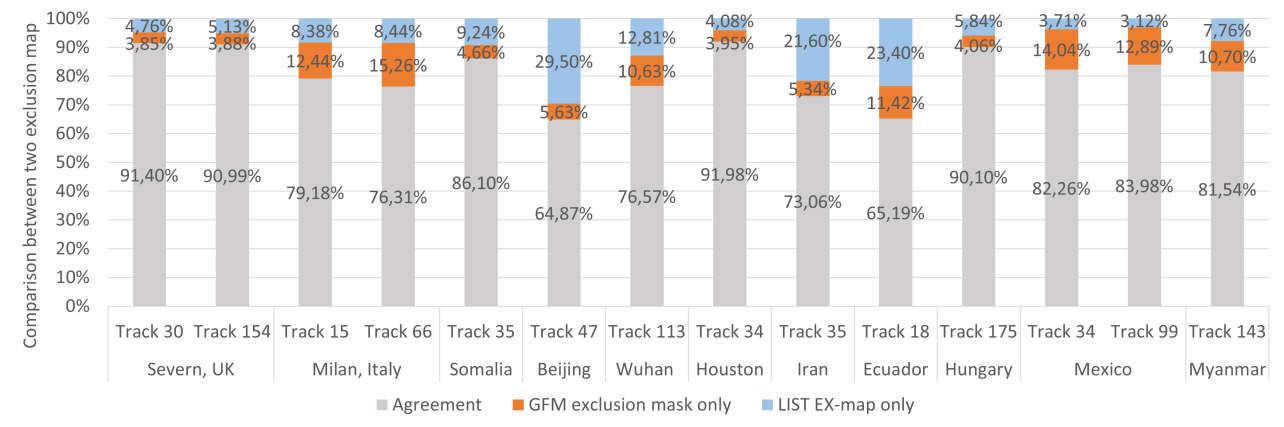

Figure 3. Cross-validation between LIST EX-map and GFM exclusion mask.

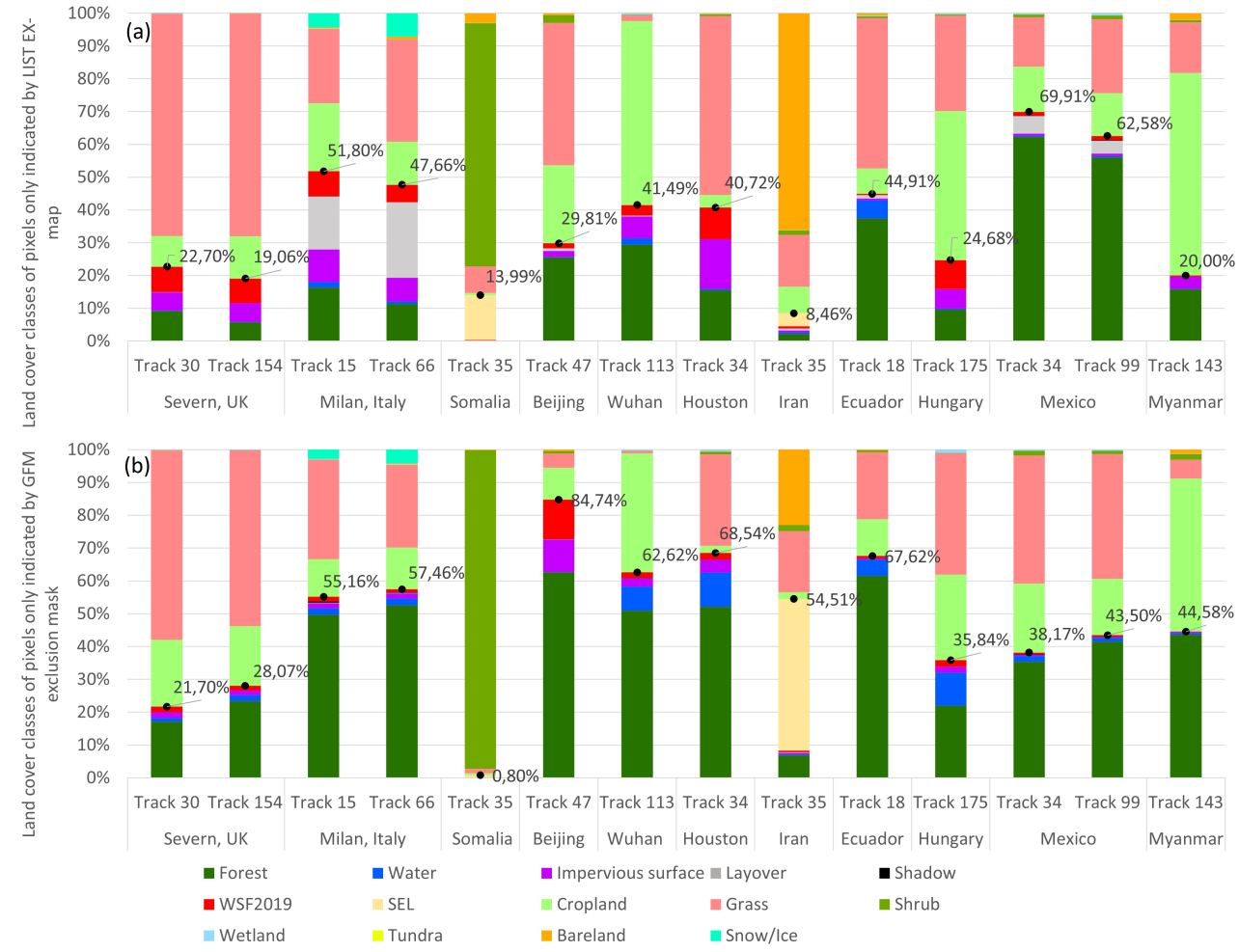

Figure 4. (a) Land cover classes of pixels included in the LIST EX-map; (b) Land cover classes of pixels included in the GFM exclusion mask.

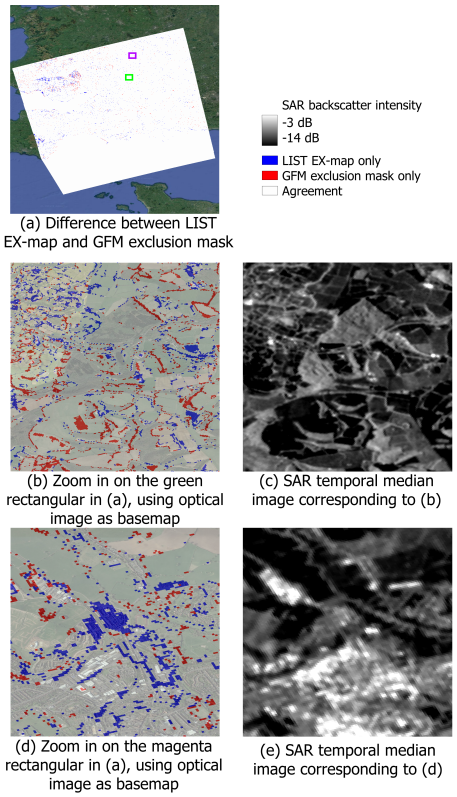

Figure 5. The disagreement between two exclusion maps in study site Severn UK.

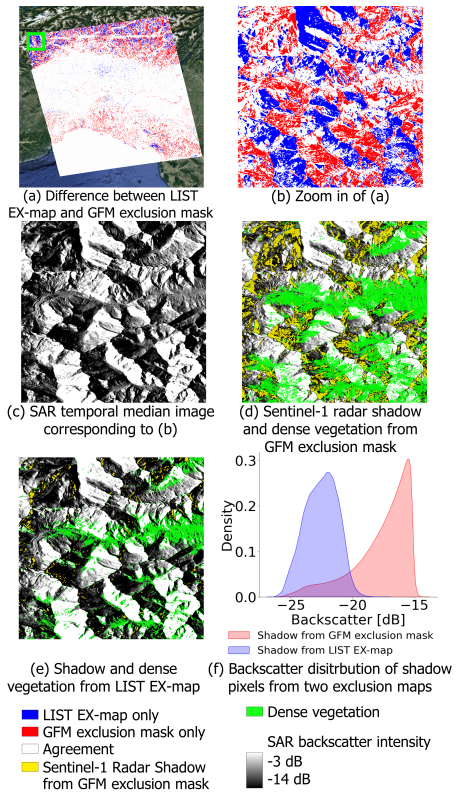

Figure 6. The disagreement between two exclusion maps in study site Milan Italy.

EX-map only identifies areas with extremely low backscatter as shadow areas (section 2.2), GFM exclusion mask is able to detect shadow areas with a relatively higher value. The explanation here is that the radar shadow layer of the GFM exclusion mask was tuned based on forest edges and riparian areas instead of mountainous regions and the topographic layovers/ shadows are expected to be included in the topographic distortion layer.

4.3.3 Study site: Beijing, China In the study site in Beijing, China, LIST EX-map covers almost the entire mountains range in the upper-left part of the scene as an LB class (Figure 7 (a)). This is due to an improper threshold being selected during LIST EX-map generation for 300 km $\times$ 300 km large tiles. More specifically, in the LIST EX-map generation algorithm, local G_i considers the relative relationship between the hot spot and the cold spot instead of their absolute relationship. Therefore, the original method was designed using 100 km $\times$ 100 km tiles in (Zhao et al., 2021) and needs to be fine-tuned to adapt to larger tiles with an optimal threshold. On the other hand, GFM exclusion mask identifies some vegetated areas as dense vegetation that may not appear dense enough from optical images (Figure 7 (b-e)). This is because the dense vegetation mask in the GFM exclusion mask is designed for the global scale product using the empirical thresholds. When applied at a regional scale, an overestimation of dense vegetation in specific areas may exist.

4.3.4 Study site: Iran Figure 8 illustrates the agreement and disagreement between two exclusion maps. It is evident that LIST EX-map exhibits an excessive number of pixels categorized as dense vegetation, which are actually bareland (Figure 8 (d) and (e)). The multi-temporal median SAR image reveals that these areas have relatively stable medium backscatter

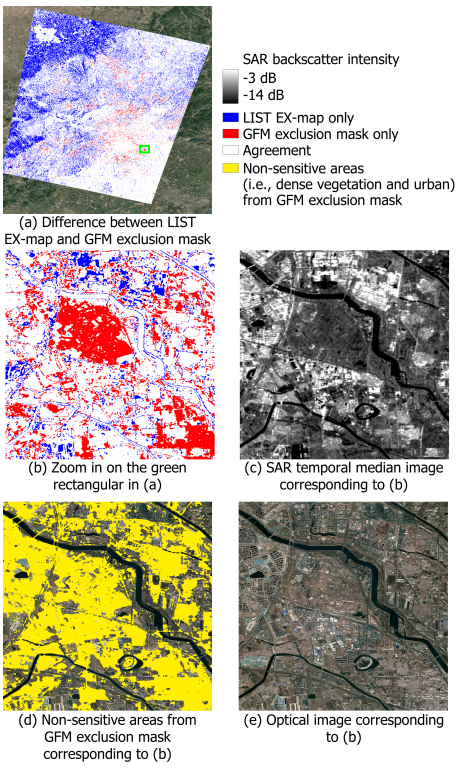

Figure 7. The disagreement between two exclusion maps in study site Beijing China.

(Figure 8 (c)), resulting in the overestimation of dense vegetation (i.e., SB class) in LIST EX-map. This suggests that the assumption made in LIST EX-map about the existence of SB class in this tile may not always valid. Therefore, the algorithm needs to be improved to ensure that SB class applies only to vegetated areas rather than bareland. Additionally, the red areas in Figure 8 (b) represent locations where GFM exclusion mask marks low backscatter areas while LIST EX-map does not. This is similar to the difference in shadows explained in section 4.3.2.

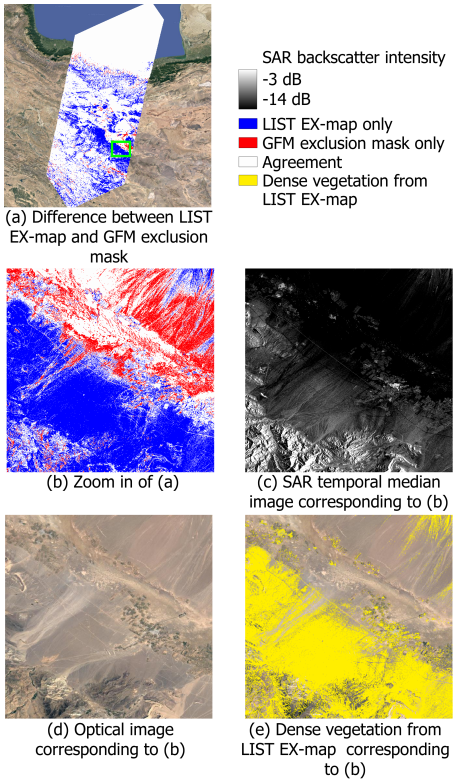

Figure 8. The disagreement between two exclusion maps in study site Iran.

4.3.5 Study site: Ecuador Figure 9 shows that LIST EX-map classifies more cropland and plantation areas as SAR-insensitive regions. For instance, plantations in Ecuador exhibit high multi-temporal medium backscatter, resulting in their categorization as HB class (i.e., layover and double-bounce effects) in LIST EX-map. On the other hand, other cropland areas with low backscatter are classified as LB class. This distinction can be seen in the example presented in Figure 9. Moreover, selecting different thresholds for different tiles during LIST EX-map generation results in a challenging seam problem when generating large-scale products, as evidenced by the clear boundary in Figure 9 (a). Furthermore, both exclusion maps in Ecuador cover a large area covered by vegetation that is difficult to evaluate using the cross-validation method employed in this study. Therefore, in the next step, the application of exclusion maps in different areas should be carried out for further evaluation, such as the flood monitoring and soil moisture monitoring over arid areas, dense vegetation.

5. CONCLUSION

This study demonstrated a detailed intercomparison between two exclusion maps - LIST EX-map and GFM exclusion mask

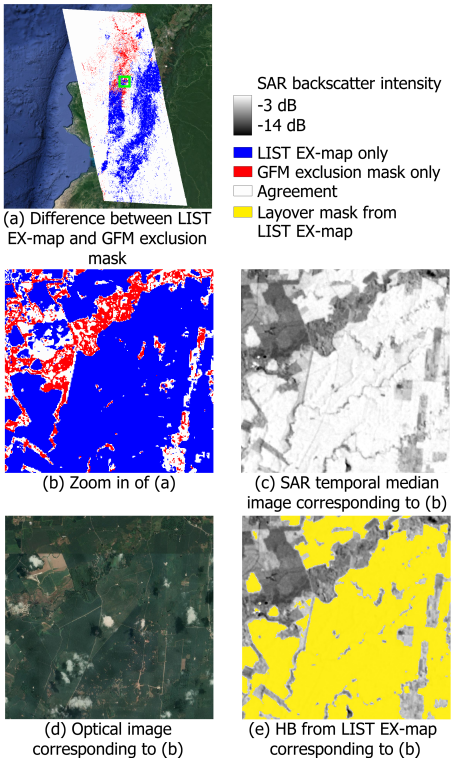

Figure 9. The disagreement between two exclusion maps in study site Ecuador.

which were designed to provide important information for large-scale SAR-derived flood mapping using Sentinel-1 data by identifying the areas where C-band Sentinel-1 SAR signal is not sensitive to surface changes. Both exclusion maps were compared with a multi-source derived reference image composed of 30m FROM-GLC land cover map, SAR simulated shadow and layover mask, 10m World Settelemt Footprint 2019 and 20m Sand Exclusion Layer to determine the land cover classes where two products agree or disagree. To better understand these two products, they were compared at 11 study sites across 5 continents with different climates and different land cover classes. The analysis led us to the following conclusions.

- A good agreement (64.87% $\sim$ 91.40%) has been found between LIST EX-map and GFM exclusion mask, despite their differing definitions. However, the LIST EX-map only considers the VV polarization, while the GFM exclusion mask uses the dual polarization of Sentinel-1 data.
- For both products, bareland and low vegetation such as cropland, grassland and shrubland are consistently classified as SAR-insensitive areas due to their similar characteristics with densely vegetated areas that have stable backscatter over time. Further discussions and analysis are still needed in the exclusion maps covering those vegetated areas.
- Radar shadow should also be further clarified for both products. In LIST EX-map, the only areas with extremely low backscatter over time are classified as radar shadows while the GFM exclusion mask identifies shadows using the backscatter thresholds of different orbits over the same regions. Thus, due to such different definitions of shadow, the LIST EX-map mainly identifies the topographic shadows while the radar shadow layer in the GFM exclusion

mask identifies the shadow from forest edges and riparian areas.

- Radar layover is identified in LIST EX-map while GFM exclusion mask uses the HAND-derived topographic distortion mask to remove the mountains and hills regions. For large-scale flood mapping applications, both products can provide additional information. However, for other applications such as soil moisture retrieval and hydrological model-based flood prediction, LIST EX-map is preferable since the SAR data may still be sensitive to surface changes in mountainous areas that are not affected by radar image distortions.

- Dense vegetation in both exclusion maps should be further examined. In LIST EX-map generation, overestimation can occur when dense vegetation is not present. The empirical thresholds used in GFM exclusion mask generation can be refined to remove some sparsely vegetated areas.

- The LIST EX-map is generated by applying an adaptive thresholding method to three multi-temporal indicators, which can be easily influenced by the size of input data. For global-scale exclusion map generation, the method of specifying thresholds by region used in GFM exclusion mask generation is worth considering. It should be noted that the global-scale GFM exclusion mask is already available as a component of the recently launched Global Flood Monitoring (GFM) (Salamon et al., 2021) component and can be accessed via the Global Flood Awareness System (GloFAS) available at `https://www.globalfloods.eu/` (accessed on 25 March 2023)).

ACKNOWLEDGEMENTS

The work of Jie Zhao and Xiao Xiang Zhu is supported by German Federal Ministry for Economic Affairs and Climate Action in the framework of the "national center of excellence ML4Earth" (grant number: 50EE2201C). This work was also supported by the Luxembourg National Research Fund (FNR) (reference: FNR PRIDE HYDRO-CSI 10623093) and the project 'Provision of an Automated, Global, Satellite-based Flood map Monitoring Product for the Copernicus Emergency Management Service (GFM) funded by the Joint Research Center of the European Commission (EC-JRC) (contract No. 939866-IPR-2020).

REFERENCES

Bauer-Marschallinger, B., Cao, S., Navacchi, C., Freeman, V., Reuß, F., Geudtner, D., Rommen, B., Vega, F. C., Snoeij, P., Attema, E. et al., 2021. The normalised Sentinel-1 Global Backscatter Model, mapping Earth's land surface with C-band microwaves. *Scientific Data*, 8(1), 277.

Bauer-Marschallinger, B., Cao, S., Tupas, M. E., Roth, F., Navacchi, C., Melzer, T., Freeman, V., Wagner, W., 2022. Satellite-Based Flood Mapping through Bayesian Inference from a Sentinel-1 SAR Datacube. *Remote Sensing*, 14(15), 3673.

Benoudjit, A., Guida, R., 2019. A novel fully automated mapping of the flood extent on SAR images using a supervised classifier. *Remote Sensing*, 11(7), 779.

Chini, M., Hostache, R., Giustarini, L., Matgen, P., 2017. A hierarchical split-based approach for parametric thresholding of SAR images: Flood inundation as a test case. *IEEE Transactions on Geoscience and Remote Sensing*, 55(12), 6975–6988.

Chow, C., Twele, A., Martinis, S., 2016. An assessment of the height above nearest drainage terrain descriptor for the thematic enhancement of automatic sar-based flood monitoring services. *Remote Sensing for Agriculture, Ecosystems, and Hydrology XVIII*, 9998, SPIE, 71–81.

GFM, 2022. Generation of the gfm product output layers: Algorithm for generating the exclusion mask. `https://extwiki.eodc.eu/GFM/PDD/GFMoutputLayers`. Accessed: 2023-03-20.

Gong, P., Wang, J., Yu, L., Zhao, Y., Zhao, Y., Liang, L., Niu, Z., Huang, X., Fu, H., Liu, S. et al., 2013. Finer resolution observation and monitoring of global land cover: First mapping results with Landsat TM and ETM+ data. *International Journal of Remote Sensing*, 34(7), 2607–2654.

JRC, 2021. Global human settlement layer understanding human presence on planet earth science based information on population and human settlements to support informed policy decisions.

Kropatsch, W. G., Strobl, D., 1990. The generation of SAR layover and shadow maps from digital elevation models. *IEEE Transactions on Geoscience and Remote Sensing*, 28(1), 98–107.

Marconcini, M., Metz-Marconcini, A., Esch, T., Gorelick, N., 2021. Understanding current trends in global urbanisation-the world settlement footprint suite. *GI_Forum*, 9(1), 33–38.

Marconcini, M., Metz-Marconcini, A., Üreyen, S., Palacios-Lopez, D., Hanke, W., Bachofer, F., Zeidler, J., Esch, T., Gorelick, N., Kakarla, A. et al., 2020. Outlining where humans live, the World Settlement Footprint 2015. *Scientific Data*, 7(1), 242.

Martinis, S., Plank, S., Ćwik, K., 2018. The use of Sentinel-1 time-series data to improve flood monitoring in arid areas. *Remote Sensing*, 10(4), 583.

Peel, M. C., Finlayson, B. L., McMahon, T. A., 2007. Updated world map of the Köppen-Geiger climate classification. *Hydrology and earth system sciences*, 11(5), 1633–1644.

Quegan, S., Le Toan, T., Yu, J. J., Ribbes, F., Floury, N., 2000. Multitemporal ERS SAR analysis applied to forest mapping. *IEEE Transactions on Geoscience and Remote Sensing*, 38(2), 741–753.

Salamon, P., Mctlormick, N., Reimer, C., Clarke, T., Bauer-Marschallinger, B., Wagner, W., Martinis, S., Chow, C., Böhnke, C., Matgen, P. et al., 2021. The new, systematic global flood monitoring product of the copernicus emergency management service. *2021 IEEE International Geoscience and Remote Sensing Symposium IGARSS*, IEEE, 1053–1056.

Wagner, W., Bauer-Marschallinger, B., Navacchi, C., Reuß, F., Cao, S., Reimer, C., Schramm, M., Briese, C., 2021. A Sentinel-1 backscatter datacube for global land monitoring applications. *Remote Sensing*, 13(22), 4622.

Zhao, J., Pelich, R., Hostache, R., Matgen, P., Cao, S., Wagner, W., Chini, M., 2021. Deriving exclusion maps from C-band SAR time-series in support of floodwater mapping. *Remote Sensing of Environment*, 265, 112668.